Enhanced photoelectrochemical water oxidation by ZnxMyO (M = Ni, Co, K, Na) nanorod arrays

Article *in* International Journal of Hydrogen Energy · January 2016

DOI: 10.1016/j.ijhydene.2015.09.116

4 authors, including:

Wei Cheat Lee
Infineon Technologies (Kulim), Malaysia
18 PUBLICATIONS **163** CITATIONS
SEE PROFILE

Giacomo Edi Canciani
Atomic Energy and Alternative Energies Commission
9 PUBLICATIONS **110** CITATIONS
SEE PROFILE

Brnyia Alwhshe
University of Sussex
1 PUBLICATION **27** CITATIONS
SEE PROFILE

INTERNATIONAL JOURNAL OF HYDROGEN ENERGY XXX (2015) 1–9

Available online at www.sciencedirect.com

ScienceDirect

journal homepage: www.elsevier.com/locate/he

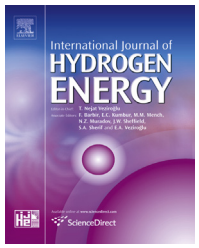

Enhanced photoelectrochemical water oxidation by Zn_xM_yO (M = Ni, Co, K, Na) nanorod arrays

Wei Cheat Lee, Giacomo E. Canciani, Brnyia O.S. Alwhshe, Qiao Chen[*]

Department of Chemistry, School of Life Sciences, University of Sussex, Brighton, BN1 9QJ, UK

ARTICLE INFO

Article history:
Received 7 July 2015
Received in revised form
23 September 2015
Accepted 27 September 2015
Available online xxx

Keywords:
Doped ZnO nanorod arrays
Chemical bath deposition
Photocatalyst
Water splitting

ABSTRACT

The present work reports a facile approach to the one-pot solution growth of vertically aligned, doped ZnO nanorod (NR) arrays by chemical bath deposition (CBD). The effects of dopant ions on the final morphologies, electronic band structures and donor densities of ZnO NRs were examined. With the introduction of dopants, the optical band gap energies of the samples were reduced. The photoelectrochemical (PEC) water splitting performances of the doped ZnO NRs were tested. When compared with pristine ZnO NRs, the doped ZnO NRs demonstrated an improvement of at least 15% in the PEC water splitting activity. Na-doped ZnO NRs was the most efficient photoanode, where its photocurrent density was 2.1 times greater than that of pristine ZnO NRs. The mechanism for improved PEC performance was proposed.

Introduction

Fossil fuels have been extensively used for several decades, resulting in an increase of greenhouse gases and toxic pollutants. As such, the development of sustainable and renewable resources is vital for the future energy security. The use of semiconductor materials for solar photoelectrochemical (PEC) and photocatalytic water splitting offer environmental friendly processes for the generation of renewable energy. Among the nanoscaled materials, 1D photocatalyts have been widely explored due to their large surface area and short diffusion lengths for photogenerated minority carriers [1–4].

Many different metal oxide nanostructures such as ZnO [5], TiO_2 [6], Fe_2O_3 [7], and WO_3 [8], have been studied for their potential application in PEC water splitting. Of these semiconductors, ZnO has been recognised as a promising photoanodic material owing to its appropriate band edges, high electron mobility, low electrical resistance and high electron-transfer efficiency [4,9]. However, the photoconversion efficiency of ZnO nanomaterials is substantially limited due to its large band gap (3.37 eV) [10]. Thus, many efforts have been focused on increasing the absorption of ZnO to the visible region, through sensitisation with dyes or quantum dots, and doping with heteroatoms [2,4,10–12].

Impurity doping has been widely investigated in the past as an effective method to increase electrical conductivity and to narrow the band gap energy of semiconductors [13–15]. So far, various types of extrinsic dopants have been introduced into ZnO in order to enhance the photoconversion efficiency [15–18]. Doped ZnO NRs have been synthesised through a variety of different techniques. Hydrothermal synthesis is one of the methods used for the growth of doped ZnO nanostructures [19,20]. Although high quality nanostructures can be achieved with this method, it is difficult to monitor and

* *Corresponding author*. Tel.: +44 1273 678492.
E-mail address: qiao.chen@sussex.ac.uk (Q. Chen).

http://dx.doi.org/10.1016/j.ijhydene.2015.09.116

control the growth process and the size of the substrate is usually limited. Ion arc implantation is another method used to introduce dopant [11]. This technique involves high vacuum environments coupled with high voltage currents, making it difficult and complex to perform. The third strategy used is chemical vapour deposition [18]. This is a complex process involving high temperatures (>600 °C), restricting the choices of substrates.

Here, we demonstrate one-pot synthesis of high quality crystallised doped ZnO NRs based on an adapted CBD method. The method allows homogenous deposition of NRs over a large surface area with a fine control on dopant concentration. In the present work, various dopants (Ni, Co, K and Na) have been introduced into ZnO nanostructures. The effects of each dopant ion on the morphologies and optical properties of the created ZnO nanostructures were investigated. The electronic structures and carrier densities were evaluated and their correlation with the PEC performance was also analysed.

Materials and methods

Preparation of catalysts

All the chemicals used were analytical grade and purchased from Sigma–Aldrich UK. The substrates, titanium plates (2×2 cm^2; Rudgwick Metals) were polished, cleaned under sonication in an isopropanol bath for 15 min, and dried in air prior to NR synthesis. ZnO NRs were prepared by CBD method as described elsewhere [5]. In this work, 0.10 M of seeding solution and 20 mM of growth solution were used. The doped ZnO nanostructures were prepared according to the same procedure with the addition of doping precursors (nickel acetate tetrahydrate, cobalt acetate tetrahydrate, potassium nitrate and sodium nitrate). Doping was carried out by adding dopant ions into the growth solution resulting in a 1:4 molar ratio of doping ions to zinc acetate. The ZnO seeded substrates were vertically positioned in glass beakers containing 100 mL of growth solution at 85 °C. After 12 h, the samples were rinsed three times with DI water, dried at room temperature, and annealed at 400 °C for 1 h.

Characterisation

The morphologies of the samples were studied by scanning electron microscopy (SEM, JSM 820M, Jeol). The crystallinity and structure orientation of the nanostructures were analysed by powder x-ray diffractometer (XRD, Siemens D500). The average diameters and average film thicknesses were measured from top- and side-view SEM images by using Image J (National Institutes of Health, USA). The light absorption spectra were recorded using a UV–Visible spectrophotometer (Thermospectronic UV 300) with samples grown on fluorine doped tin oxide (FTO) glass substrates (supplied by Sigma–Aldrich UK) under identical conditions. The actual dopant concentrations were measured using inductively coupled plasma mass spectroscopy (ICP-MS; Agilent 7500ce).

Photocatalytic water splitting

The PEC water splitting was measured using a standard three-electrode configuration in a 1.0 M KOH electrolyte (pH 13.6). A platinum foil was used as counter electrode and a KCl saturated Ag/AgCl electrode was used as a reference. A USB potentiostat (eDAQ) was used to control and record the photocurrent as a function of electrochemical potential. Sunlight was simulated with a 300W xenon arc lamp with an AM1.5 G filter and the output light power density was adjusted to 100 mW cm^{-2}. The optical power density was calibrated by a power meter (Newport 1830-C) with a wide band sensor (Newport 818-UV attenuated). Electrochemical impedance spectroscopy (EIS; Palmsens 3.0) measurements were carried out in either 0.5 M Na_2SO_4 solution (pH 6.8) or 1.0 M KOH solution (pH 13.6) at a fixed frequency of 1 kHz, the amplitude of the sinusoidal wave was set at 10 mV.

Results and discussion

The top view morphologies of the synthesised pure ZnO and doped ZnO NRs are shown in Fig. 1. Fig. 1B–E reveal the morphologies of the NRs doped with Ni (B), Co (C), K (D) and Na ions (E). Although the typical hexagonal cross sections are still observed, the density and diameter of the doped NRs are varied depending on the dopant. The morphologies of Na-, Co- and Ni-doped ZnO NRs are significantly affected the coalescence of the NRs. For the Ni-doped ZnO sample, the formed rods are much bigger in diameter than any other NRs, resulting in a densely packed structure (Fig. 1B). Meanwhile, the hexagonal cross sections of the Co and Na-doped ZnO NRs (Fig. 1C and E) are less well defined as the result of coalescence of the adjacent NRs. The average diameters of the undoped, Ni-, Co-, K- and Na-doped ZnO NRs were measured (based on 100 measurements for each sample) to be 160 ± 22, 440 ± 66, 200 ± 24, 180 ± 21 and 170 ± 24 nm, respectively.

In addition, the dopants can also affect the NR length, as presented in Fig. 2. The average lengths of the undoped, Ni-, Co-, K- and Na-doped ZnO NRs were determined to be 4.0, 2.2, 3.1, 3.6 and 3.8 μm, respectively. The length of the NRs is directly correlated to the diameter of the NRs, ruled by the mass conservation. For the Na- and K-doped ZnO samples, the average lengths of the NRs are slightly shorter, while their diameters are slightly larger than those of pristine ZnO NRs. The extreme example is the Ni-doped ZnO NRs which are much shorter, and their diameters are much larger than the pristine ZnO NRs. Quantitative analysis reveals that the length of the Co-doped ZnO NRs is about ~77.5% of the pristine ZnO NRs, while the length of the Ni-doped ZnO NRs is about 50% of the pristine ZnO NRs.

The large diameter is consistent with the shorter length of doped ZnO NRs. In order to establish the NR surface density, the volume (V) of individual NR was calculated using its averaged radius and length. The results present in Table 1 reveal that most of doped NRs have similar single rod volume, except for the Ni-doped ZnO sample which has a volume 3–4 times larger. This suggests that the density of the NRs was determined by the seeding process and maintained as

Please cite this article in press as: Lee WC, et al., Enhanced photoelectrochemical water oxidation by Zn_xM_yO (M = Ni, Co, K, Na) nanorod arrays, International Journal of Hydrogen Energy (2015), http://dx.doi.org/10.1016/j.ijhydene.2015.09.116

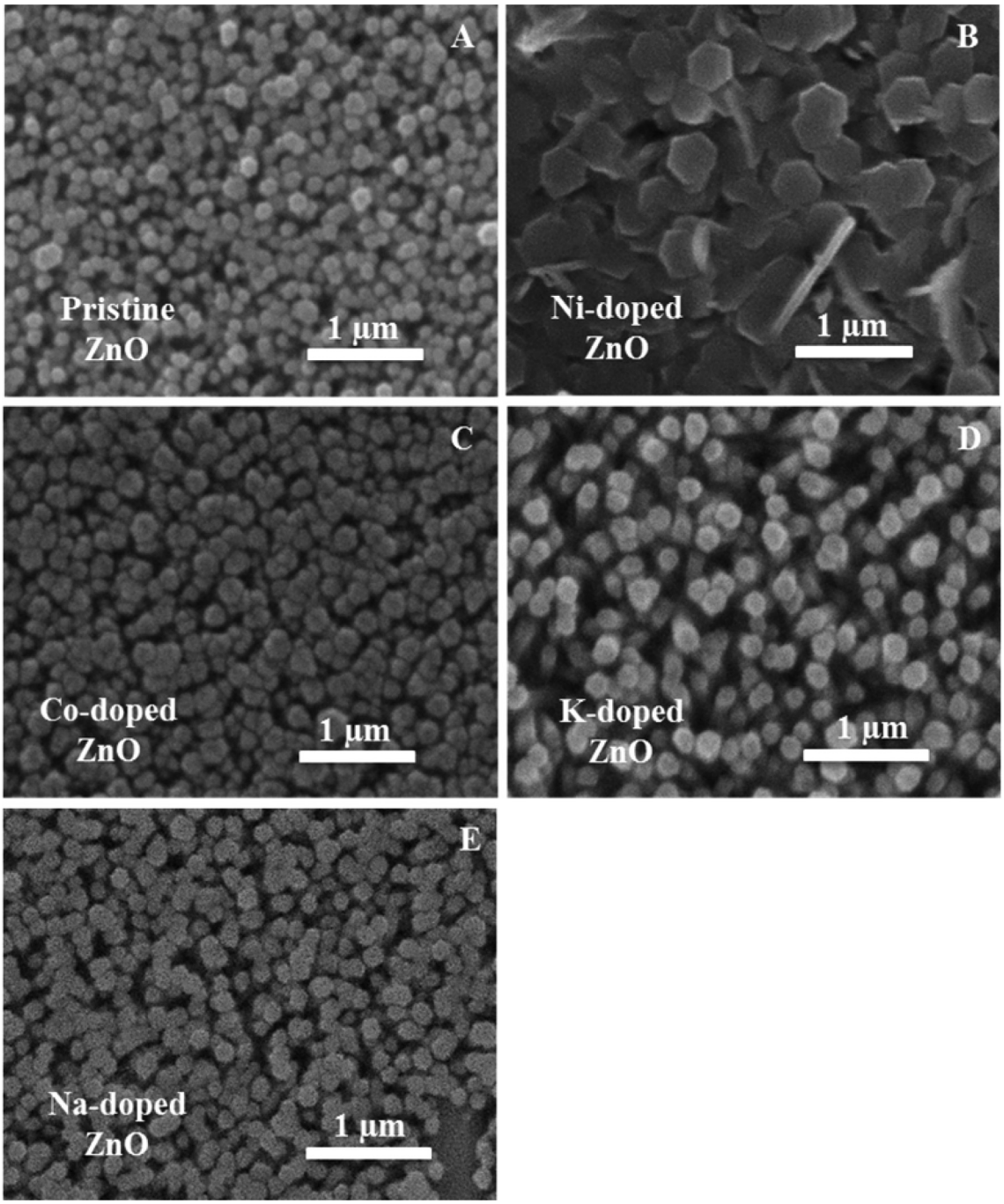

Fig. 1 – Top view SEM images of (A) undoped, (B) Ni-, (C) Co-, (D) K- and (E) Na-doped ZnO NRs.

constant for all the doped ZnO NRs. For Ni-doped ZnO NRs, every 3 or 4 NRs were coalesced, resulting in a large volume and large diameter of each rod.

The change in the NR shape aspect ratio can be attributed to the dopant ions suppressing the growth of ZnO NRs along the (002) face. The doping ions in the nutrient solutions form charged complex ions (cation or anion) which will selectively interact with the ZnO facets leading to an alteration of the NR growth kinetics [21,22]. Since the (002) plane of ZnO is negatively charged in aqueous solution [21], this suggests that Ni^{2+}, Co^{2+}, K^{+} and Na^{+} ions predominantly formed positively charged complexes in alkaline solutions, which will be attracted onto the (002) plane, inhibiting NR growth along the [0001] direction.

The surface area to volume ratio (*SAVR*) determines the geometry effects on the reaction kinetics for gas or liquid at solid surface [5]. Based on the measured morphological dimensions in Table 1, the surface area to volume ratio (*SAVR*) values were calculated to be 0.0181, 0.0110, 0.0175, 0.0184 and 0.0194 nm^{-1} for pristine ZnO, Ni-, Co-, K- and Na-doped ZnO NR arrays, respectively. The higher surface area density offers more reaction centres which can improve the reaction kinetics.

Please cite this article in press as: Lee WC, et al., Enhanced photoelectrochemical water oxidation by Zn_xM_yO (M = Ni, Co, K, Na) nanorod arrays, International Journal of Hydrogen Energy (2015), http://dx.doi.org/10.1016/j.ijhydene.2015.09.116

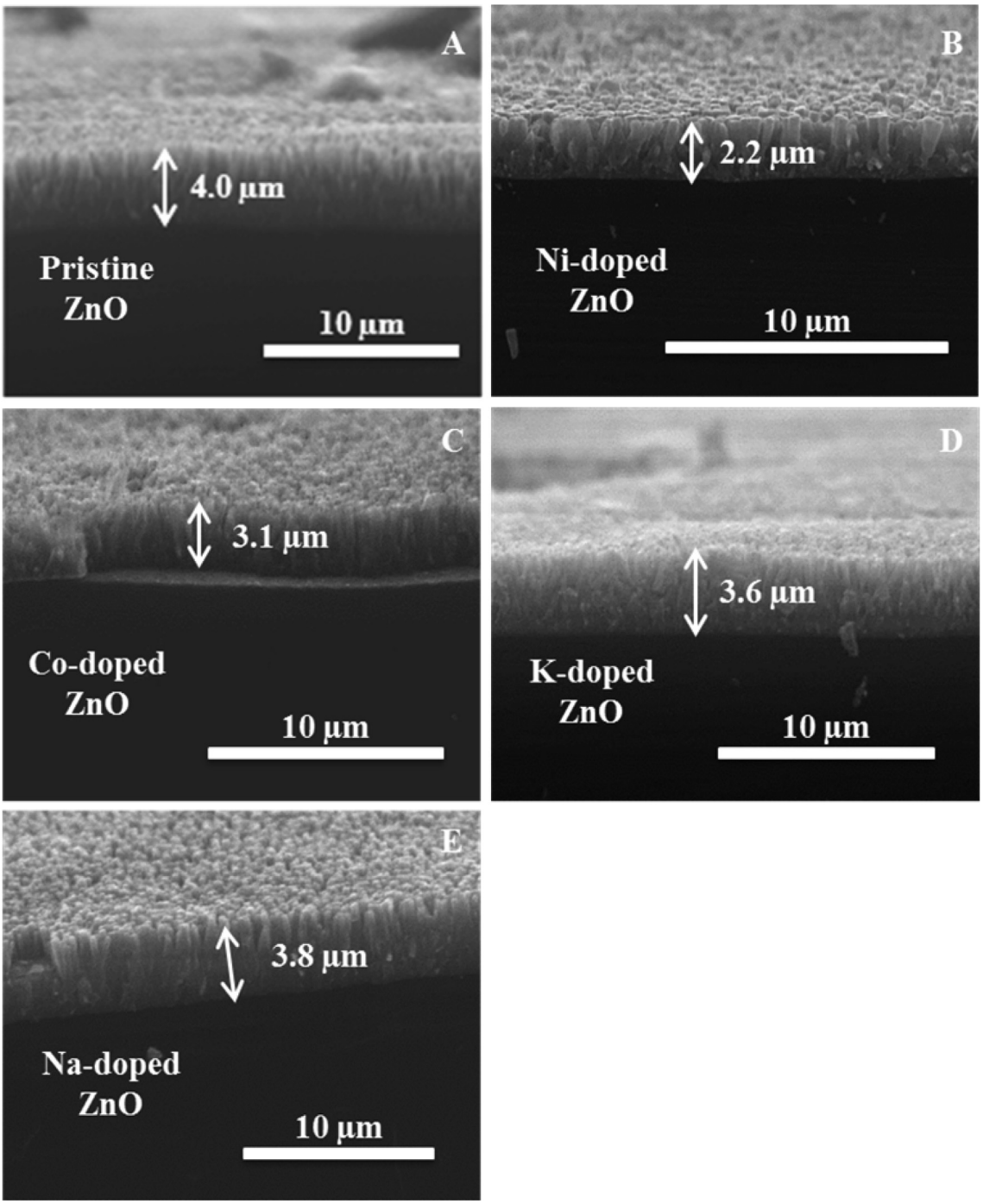

Fig. 2 – Side view SEM images of (A) undoped, (B) Ni-, (C) Co-, (D) K- and (E) Na-doped ZnO NRs.

Table 1 – Morphological parameters, volume and surface area to volume ratio (SAVR) of ZnO NRs.

NR samples	Dimensions (μm)		V (μm^3)	SAVR (nm^{-1})
	Radius	Length		
Pristine ZnO	0.08	4.0	0.0665	0.0181
Ni-doped ZnO	0.22	2.2	0.2766	0.0110
Co-doped ZnO	0.10	3.1	0.0805	0.0175
K-doped ZnO	0.09	3.6	0.0799	0.0184
Na-doped ZnO	0.09	3.8	0.0713	0.0194

The powder XRD patterns of the as-grown ZnO NRs and doped ZnO NRs were analysed based on the standard XRD database for wurtzite ZnO (JCPDS 36-1451) and alpha-titanium (JCPDS 44-1294). As shown in Fig. 3A–E, all the XRD diffraction peaks were indexed to the typical wurtzite hexagonal phase of ZnO dominated by the (002) diffraction and there is no dopant metal oxides phases were observed. This indicates either the dopant concentrations were too low or the dopants were homogenously distributed into the ZnO NRs. It is important to note that, when compared to pristine ZnO, the (002) peak positions of the Na- and K-doped ZnO samples are having an

Please cite this article in press as: Lee WC, et al., Enhanced photoelectrochemical water oxidation by Zn_xM_yO (M = Ni, Co, K, Na) nanorod arrays, International Journal of Hydrogen Energy (2015), http://dx.doi.org/10.1016/j.ijhydene.2015.09.116

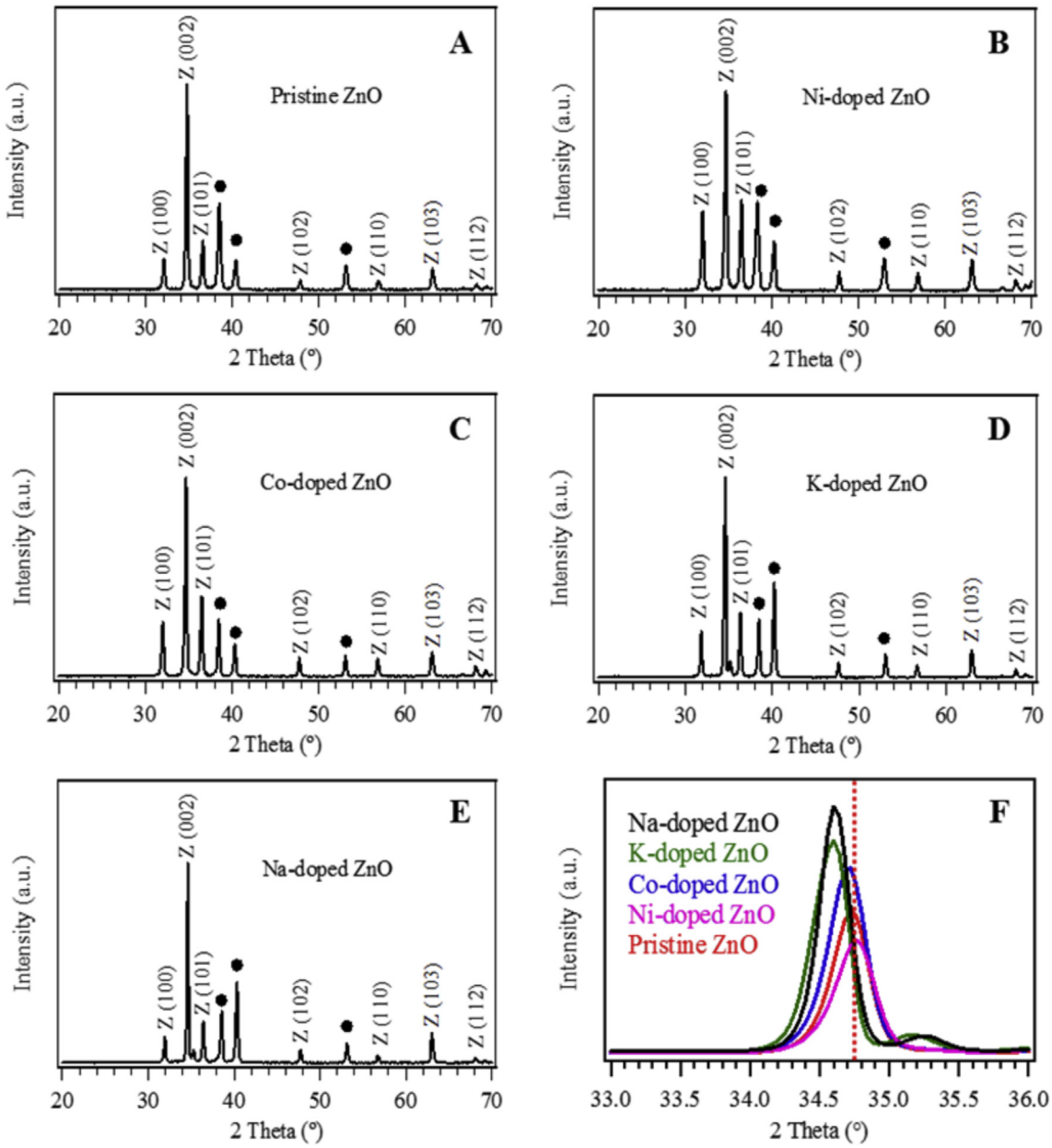

Fig. 3 – XRD patterns of (A) undoped, (B) Ni-, (C) Co-, (D) K- and (E) Na-doped ZnO NRs. The miller indices of crystal planes are labelled where Z and ● are ZnO and titanium, respectively. (F) Enlarged (002) diffraction peaks of pristine and doped ZnO NRs.

obvious shift toward lower angle (Fig. 3F), while the Ni- and Co-doped ZnO samples show very little shift. The peak shift can be attributed to the distortion of the ZnO lattice after interstitial doping. The c-lattice constants [23] of undoped, Ni-, Co-, K- and Na-doped ZnO NRs were calculated to be 5.163, 5.160, 5.162, 5.181 and 5.179 Å, respectively. The variation of the lattice constants is directly determined by the ion radius of the dopant. The expansion of the ZnO lattice for K- and Na-doped ZnO samples were due to the larger ionic radii of K^+ (1.51 Å) and Na^+ (1.18 Å) with respect to the Zn^{2+} (0.74 Å) [24]. The obtained results are consistent with the previous findings [13,25]. For Co- and Ni-doped ZnO samples, the ionic radii of Ni^{2+} (0.69 Å) and Co^{2+} (0.72 Å) [26] are slightly smaller than the ionic radius of Zn^{2+}, thus the substitution of Ni^{2+} or Co^{2+} ions into the zinc sites will cause a small reduction of the ZnO lattice. Similar XRD spectra were also found in recent investigation for the solution growth of Ni- and Co-doped ZnO nanostructures [27,28].

In order to determine the actual dopant concentration in the ZnO crystal, ICP-MS measurements were carried out (Table 2). It is noticeable that the actual dopant/Zn molar percentages are about 10% of that in the nutrient solutions. The low-level of doping efficiency can be attributed to the solubility of these dopants in ZnO [14,27]. The dopant solubility increases with increasing the operating temperature since the diffusion of the dopant ions into the ZnO crystals is favoured at high temperature [29]. In the present work, the CBD reacts at a rather low temperature (~85 °C), thus the

Please cite this article in press as: Lee WC, et al., Enhanced photoelectrochemical water oxidation by Zn_xM_yO (M = Ni, Co, K, Na) nanorod arrays, International Journal of Hydrogen Energy (2015), http://dx.doi.org/10.1016/j.ijhydene.2015.09.116

Table 2 – ICP-MS analysis of doped ZnO NRs.

NR samples	Dopant concentration (%)		Doping efficiency (%)
	Solution	Film	
Ni-doped ZnO	25.0	3.23 ± 0.26	12.92
Co-doped ZnO	25.0	2.95 ± 0.28	11.80
K-doped ZnO	25.0	1.98 ± 0.36	7.92
Na-doped ZnO	25.0	2.17 ± 0.42	8.68

solubilities of the dopant ions are expected to be much lower. Similar low-level doping behaviour for transition metal ion doping in ZnO nanocrystals has been reported [14,30]. In comparison with Na and K, Co and Ni have achieved relatively higher dopant concentrations. This observation can be explained by the high binding energy of the Co^{2+} and Ni^{2+} and large ion radii of Na^{+} and K^{+}. This is consistent with the observation of morphology variation, lattice constants enlargement and crystal textures for our Ni-, Co-, K- and Na-doped ZnO NRs.

The effect of doping on the light absorption of ZnO NRs was investigated using a UV–Vis spectrophotometer. Fig. 4A reveals the UV–Vis absorption onset of the doped ZnO NRs is shifted to a longer wavelength (>400 nm) when compared to the pristine ZnO NRs (~387 nm). The red shift (in the web version) could significantly enhance the absorption of solar energy in the visible region, indicating reduced optical band gaps. The optical band gap was determined by the Tauc equation from the extinction coefficient (α) as a function of photon energy ($h\nu$) [31], as presented in Fig. 4B. The measured absorption spectrum has some background in the long wavelength region (450–600 nm), which is due to either light scattering from micro texture of the NRs or the light absorption by the defects state. Such background was corrected before the Tauc plots were made. The linear nature of the Tauc plots at the absorption edges confirms that all the samples are direct band gap semiconductors. The band gap energies of Ni-, Co-, K- and Na-doped ZnO NRs were determined to be 3.17, 3.15, 3.16 and 3.14 eV, smaller than 3.28 eV of the pristine ZnO.

The reduction of band gap energies could be due to the creation of defect centres, such as oxygen vacancies [32], or by the formation of dopant states inside the band gap of ZnO [13,33]. The structure disordering and density of defects can also be reflected by the light absorption below the optical gap, defined as Urbach tail. The Urbach energy (E_u) can be obtained from the inverse of the slope of ln α as a function of $h\nu$ [34], as shown in Fig. 5. The E_u values of undoped, Ni-, Co-, K- and Na-doped ZnO NRs were 94.5, 105.8, 112.6, 163.2 and 169.4 meV, respectively. The obtained E_u value of pristine ZnO NRs is comparable with the reported value [15]. It is important to note that all the doped ZnO NRs are having a higher E_u value as compared to that of pure ZnO. The larger the E_u value indicates an increased in the structural disorder and the number of defects in the doped nanomaterials [15].

The PEC water splitting performances of the undoped and doped ZnO NRs were investigated. Fig. 6 shows the photocurrents generated from pure ZnO, Ni-, Co-, K- and Na-doped ZnO between potentials of −0.5 and 1.0 $V_{Ag/AgCl}$ together with the dark currents measured in 1.0 M KOH electrolyte (pH 13.6). For all samples, the dark current are too small to be distinguishable when the potential is below 0.87 $V_{Ag/AgCl}$, above which the electrochemical water oxidation starts to be observable from the increase of the anodic dark current. In comparison to the pure ZnO NRs photoanode, it is obvious that the doped ZnO NRs demonstrated a significant

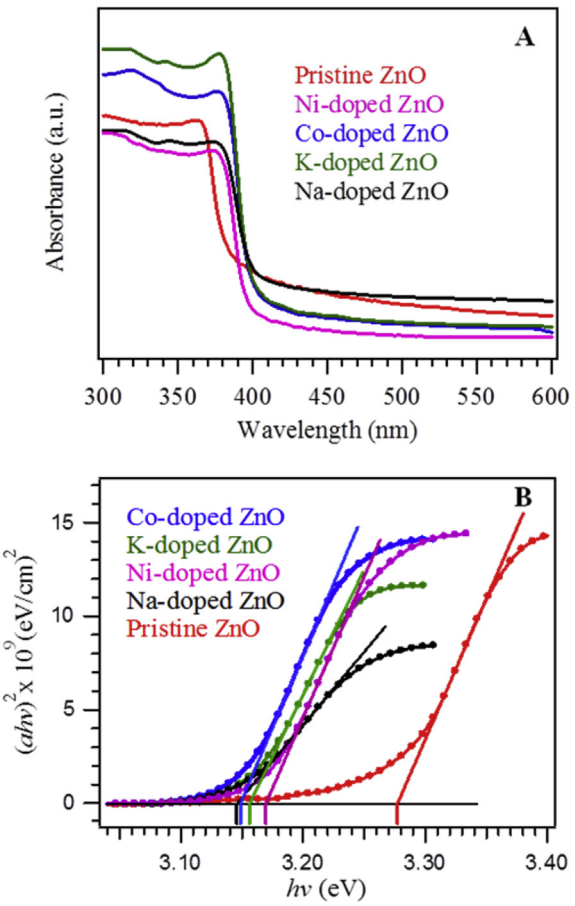

Fig. 4 – (A) UV–Vis absorption spectra and (B) Tauc plots of undoped and doped ZnO NRs.

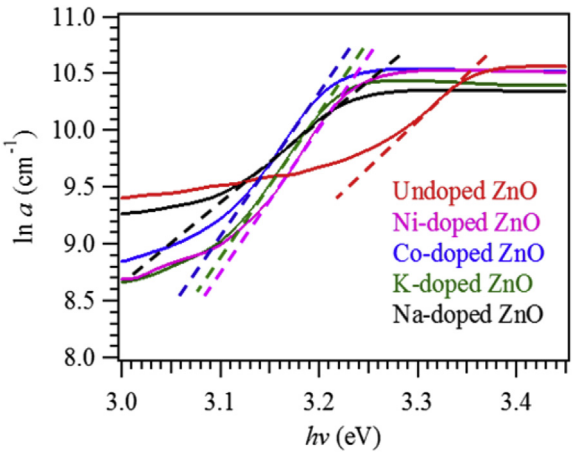

Fig. 5 – Plots of ln α as a function of photon energy for undoped and doped ZnO NRs.

Please cite this article in press as: Lee WC, et al., Enhanced photoelectrochemical water oxidation by Zn_xM_yO (M = Ni, Co, K, Na) nanorod arrays, International Journal of Hydrogen Energy (2015), http://dx.doi.org/10.1016/j.ijhydene.2015.09.116

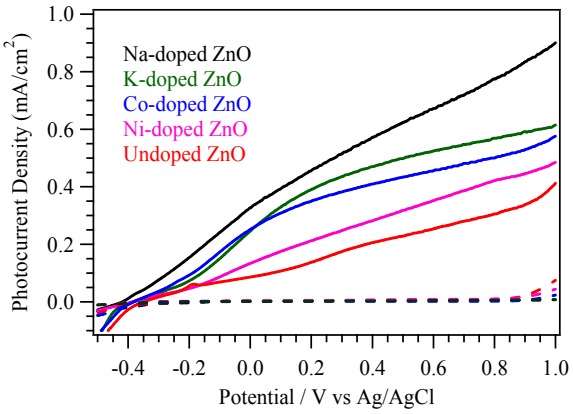

Fig. 6 – Photocurrents generated from pristine and doped ZnO NRs. The dotted lines are their corresponding dark current.

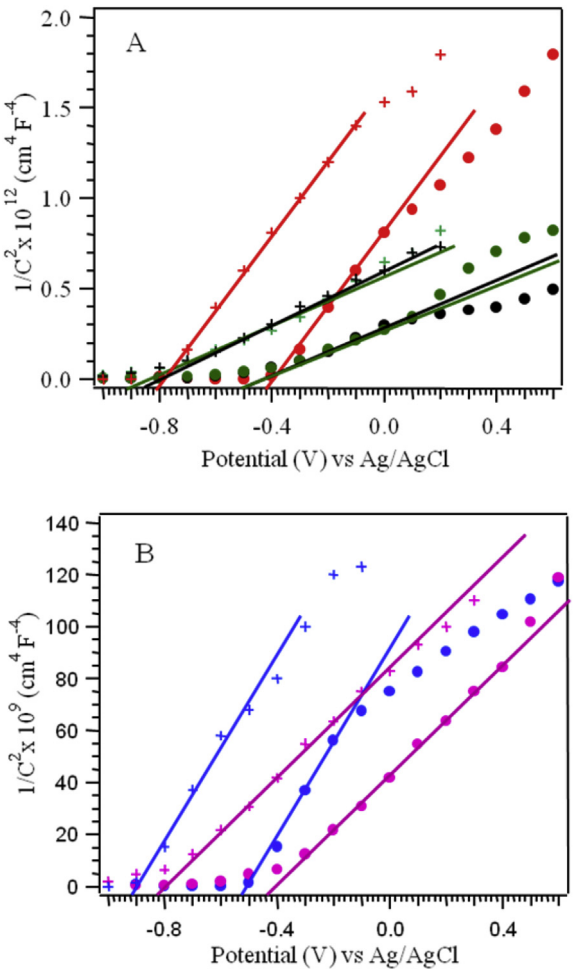

Fig. 7 – M–S plots of (A) undoped (red), K- (green) and Na-doped (black) ZnO NRs and (B) Co- (blue) and Ni-doped (pink) ZnO NRs. In each plot the data was measured at either pH = 6.8 (●) or pH = 13.6 (+). (For interpretation of the references to colour in this figure legend, the reader is referred to the web version of this article.)

improvement in the photocurrent density. At a typical potential of 1.0 $V_{Ag/AgCl}$, the photocurrents generated from pure ZnO, Ni-, Co-, K- and Na-doped ZnO NRs photoanodes were 0.42, 0.48, 0.58, 0.62 and 0.90 mA cm^{-2}, respectively. This represents a ~114% photocurrent density increment for the Na doped ZnO NRs. It is worth noting that the onset potentials of the doped ZnO NR anodes are more negative than that of pristine ZnO NR anode, which are −0.35, −0.39, −0.38, −0.39 and −0.42 $V_{Ag/AgCl}$ for pure ZnO, Ni-, Co-, K- and Na-doped ZnO NRs, respectively. The more negative onset potentials of doped ZnO NRs can be attributed to the created defects (oxygen vacancies) of the electrode after the introduction of dopants, causing in lowering the kinetic barrier to interfacial charge transfer [4]. Therefore, it requires a smaller overpotential for water oxidation. We are also aware of the presence of cathodic photocurrent at voltages below the onset potentials. Such cathodic photocurrents are caused by reduction processes at the anodes, which can be either contributed from the reduction of water or the reduction of dopant species at the electrode/electrolyte interfaces. However, as such cathodic photocurrent was very low for undoped ZnO NRs, it is likely that the reduction of the dopants is the source of the cathodic photocurrent. Such cathodic photocurrent has also been observed from other doped ZnO nanomaterials [4,35].

In order to establish the correlation between the charge carrier density and the photocatalytic performance, EIS measurements were carried out either in 0.5 M of Na_2SO_4 (pH 6.8) or in 1.0 M KOH (pH 13.6) in the dark. Fig. 7 shows all the samples have a positive slope in the Mott–Schottky (M–S) plots, which confirm the n-type semiconductor behaviour of the electrodes. The flat-band potential, V_{FB}, of the photoanodes can be obtained by M–S analysis by the linear extrapolation of *x*-intercepts in M–S plots [36]. At pH 6.8, the V_{FB} values of undoped, Ni-, Co-, K- and Na-doped ZnO NRs were −0.41, −0.44, −0.54, −0.52 and −0.52 $V_{Ag/AgCl}$. At pH 13.6, these V_{FB} values shift towards the negative potential to −0.80, −0.83, −0.92, −0.92 and −0.86 $V_{Ag/AgCl}$ respectively. The average difference of the V_{FB} between pH 6.8 and 13.6 is about 0.38 V, which is in reasonable agreement with the Nernst equation. The more negative V_{FB} values suggest that the charge separation of the doped ZnO samples is improved. This can be accredited to the doped ZnO samples have a lower potential barrier to overcome, resulting in a reduction of the charge transfer resistance. It is important to note that the obtained onset potentials are more positive than the V_{FB} values. The difference between the V_{FB} and the onset potential from PEC is defined as the overpotential in the oxygen evolution reaction (OER), caused by the interfacial charge transport limitations of the samples [37]. Surface modification with lower overpotential in OER will help to improve the water oxidation efficiency by moving the onset potential towards the V_{FB}. The OER overpotentials are estimated to be 0.45, 0.44, 0.54, 0.53 and 0.44 V for undoped, Ni-, Co-, K- and Na-doped ZnO NR.

The slopes of the M–S plots can be used to derive the charge carrier density of the photoanodes [11]. It is clear that pH of the electrolyte has very little effects on the slope of the M–S plots, therefore it is confident to assume that the defects and carrier density are the dominant factors that determine the slope in the M–S plots and there is no significant change of

Please cite this article in press as: Lee WC, et al., Enhanced photoelectrochemical water oxidation by Zn_xM_yO (M = Ni, Co, K, Na) nanorod arrays, International Journal of Hydrogen Energy (2015), http://dx.doi.org/10.1016/j.ijhydene.2015.09.116

the surface states at different pH. Fig. 7 shows the doped ZnO electrodes have a substantially smaller gradient with respect to the pristine ZnO electrode, which implies the donor densities of the doped ZnO samples are increased. For ZnO, with a relative dielectric constant value of 10 [38], the donor densities of pure ZnO, Ni-, Co-, K- and Na-doped ZnO were calculated to be 7.61×10^{18}, 1.34×10^{20}, 1.05×10^{20}, 2.48×10^{19} and 2.20×10^{19} cm^{-3}, respectively.

Fig. 8 shows the approximate band edge positions (at pH = 13.6) of undoped and doped ZnO based on the above measured flat-band potentials, which are the differences between Fermi levels and water-reduction potential. Here we assumed that Fermi levels were about 0.3 eV below the conduction band edge for lightly doped n-type ZnO [39,40]. The calculated conduction band edges are at −1.10, −1.13, −1.22, −1.22 and −1.16 V_{NHE} for undoped, Ni-, Co-, K- and Na-doped ZnO NRs, respectively, while the H^+/H_2 reduction potential is at −0.80 V_{NHE}. Therefore, all the conduction band edges are more negative than the hydrogen redox potential. The valence band edge was determined by combining the band gap energies from the Taus plots (Fig. 4B). Fig. 8 shows that although there is no significant difference between the band edges of the ZnO samples, the conduction band edges of doped ZnO were all shifted towards negative potential. Such shift could slightly improve the PEC performance.

The higher PEC performances of the doped ZnO NRs, relative to the pure ZnO NRs, can be explained in several ways. The doping is normally associated with crystal defects and domain boundaries. XRD spectra reveal that Na- and K-doped ZnO crystals have the largest lattice distortion. The presence of defects and domain boundaries could form charge trapping centres, which could improve the charge separation at the interface of semiconductor and electrolyte [2], and thus enhanced the PEC water splitting performances. The decreased band gap energy of doped ZnO means photoexcitation can be effectively extended towards the visible range. The Na-doped ZnO NRs give the smallest band gap with the highest photocurrent, although the Na dopant concentration and associated charge carrier density were relative low. This suggests that in our work, the band gap reduction is more important than the doping level. A quantitative study of the effects of doping level on the PEC activity will be carried out in the future work. The improved PEC performance could also be correlated to the negative shift of the onset potentials of doped ZnO within which the Na-doped ZnO shows the most negative onset potential with the highest photocurrent. The onset potential of an n-type semiconductor is defined by the flat-band potential with the correction of overpotential. For Na-doped ZnO, although its flat-band potential is not the most negative, its overpotential (0.44 V) is the lowest of all the tested samples. This indicates that the presence of crystal defects and Na dopant could improve the water oxidation and oxygen evolution with low reaction energy barrier. Finally, the PEC water splitting activity can also be affected by nanomorphology. The highest *SAVR* values of Na- and K-doped ZnO NR arrays are consistent with the highest photocurrent densities from those samples.

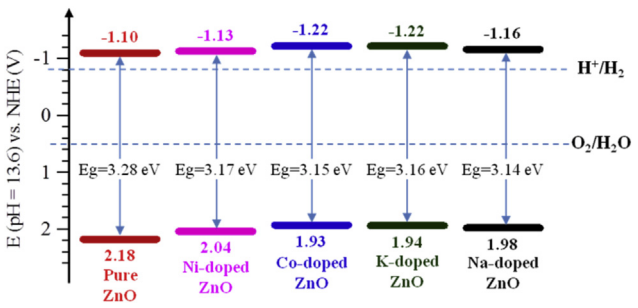

Fig. 8 – Energy diagrams for doped and undoped ZnO NRs. The redox potentials for water oxidation and H^+ reduction were also labelled.

Conclusions

Doped ZnO NRs were successfully created through the one-pot aqueous CBD method. The surface morphology of ZnO nanostructures was strongly affected by the types of charged complex ions formed by the dopants, which will either increase or decrease the NR aspect ratio. The UV–Vis absorption spectra revealed that all the doped ZnO samples possessed smaller optical band gap energy than that of pure ZnO NRs. The PEC measurements revealed that the Na-doped ZnO NRs anode exhibited the highest PEC water splitting photocurrent, which is 2.1 times more than the pristine ZnO NRs anode. Possible mechanisms for the high efficiency were also discussed.

Acknowledgements

W.C. Lee would like to thank Public Service Department of Malaysia (JPA) for his scholarship.

REFERENCES

[1] Wang GM, Wang HY, Ling YC, Tang YC, Yang XY, Fitzmorris RC, et al. Hydrogen-treated TiO_2 nanowire arrays for photoelectrochemical water splitting. Nano Lett 2011;11:3026–33.
[2] Lin Y-G, Hsu Y-K, Chen Y-C, Lee B-W, Hwang J-S, Chen L-C, et al. Cobalt-phosphate-assisted photoelectrochemical water oxidation by arrays of molybdenum-doped zinc oxide nanorods. ChemSusChem 2014;7:2748–54.
[3] Hisatomi T, Kubota J, Domen K. Recent advances in semiconductors for photocatalytic and photoelectrochemical water splitting. Chem Soc Rev 2014;43:7520–35.
[4] Chen CK, Shen YP, Chen HM, Chen CJ, Chan TS, Lee JF, et al. Quantum-dot-sensitized nitrogen-doped ZnO for efficient photoelectrochemical water splitting. Eur J Inorg Chem 2014;2014:773–9.
[5] Lee WC, Fang YX, Kler R, Canciani GE, Draper TC, Al-Abdullah ZTY, et al. Marangoni ring-templated vertically aligned ZnO nanotube arrays with enhanced photocatalytic hydrogen production. Mater Chem Phys 2015;149–150:12–6.
[6] Bettini LG, Della Foglia F, Milani P, Piseri P. Nanostructured carbon substrate improves the photoelectrochemical water splitting activity of cluster-assembled TiO_2 thin films. Int J Hydrogen Energy 2015;40:6013–20.

Please cite this article in press as: Lee WC, et al., Enhanced photoelectrochemical water oxidation by Zn_xM_yO (M = Ni, Co, K, Na) nanorod arrays, International Journal of Hydrogen Energy (2015), http://dx.doi.org/10.1016/j.ijhydene.2015.09.116

[7] Lee WJ, Shinde PS, Go GH, Doh CH. Cathodic shift and improved photocurrent performance of cost-effective Fe_2O_3 photoanodes. Int J Hydrogen Energy 2014;39:5575–9.
[8] Fang YX, Lee WC, Canciani CE, Draper TC, Al-Bawi ZF, Bedi JS, et al. Thickness control in electrophoretic deposition of WO_3 nanofiber thin films for solar water splitting. Mat Sci Eng B Solid 2015. http://dx.doi.org/10.1016/j.mseb.2015.09.005.
[9] Huang MH, Mao S, Feick H, Yan HQ, Wu YY, Kind H, et al. Room-temperature ultraviolet nanowire nanolasers. Science 2001;292:1897–9.
[10] Lin Y-G, Hsu Y-K, Chen Y-C, Wang S-B, Miller JT, Chen L-C, et al. Plasmonic Ag@Ag3(PO4)1-x nanoparticle photosensitized ZnO nanorod-array photoanodes for water oxidation. Energy Environ Sci 2012;5:8917–22.
[11] Wang M, Ren F, Cai GX, Liu YC, Shen SH, Guo LJ. Activating ZnO nanorod photoanodes in visible light by Cu ion implantation. Nano Res 2014;7:353–64.
[12] Lu YH, Lin WH, Yang CY, Chiu YH, Pu YC, Lee MH, et al. A facile green antisolvent approach to Cu^{2+}-doped ZnO nanocrystals with visible-light-responsive photoactivities. Nanoscale 2014;6:8796–803.
[13] Bharathi V, Sivakumar M, Udayabhaskar R, Takebe H, Karthikeyan B. Optical, structural, enhanced local vibrational and fluorescence properties in K-doped ZnO nanostructures. Appl Phys A Mater 2014;116:395–401.
[14] Panigrahy B, Aslam M, Bahadur D. Aqueous synthesis of Mn- and Co-doped ZnO nanorods. J Phys Chem C 2010;114:11758–63.
[15] Ilican S. Effect of Na doping on the microstructures and optical properties of ZnO nanorods. J Alloy Compd 2013;553:225–32.
[16] Sin JC, Lam SM, Lee KT, Mohamed AR. Preparation of rare earth-doped ZnO hierarchical micro/nanospheres and their enhanced photocatalytic activity under visible light irradiation. Ceram Int 2014;40:5431–40.
[17] Wang F, Seo J-H, Li Z, Kvit AV, Ma Z, Wang X. Cl-doped ZnO nanowires with metallic conductivity and their application for high-performance photoelectrochemical electrodes. ACS Appl Mater Interfaces 2014;6:1288–93.
[18] Anusha M, Arivuoli D. High intense violet luminescence in fluorine doped zinc oxide (FZO) thin films deposited by aerosol assisted CVD. J Alloy Compd 2013;580:131–6.
[19] Downing JM, Ryan MP, McLachlan MA. Hydrothermal growth of ZnO nanorods: the role of KCl in controlling rod morphology. Thin Solid Films 2013;539:18–22.
[20] Sheng WJ, Sun B, Shi TL, Tan XH, Peng ZC, Liao GL. Quantum dot-sensitized hierarchical micro/nanowire architecture for photoelectrochemical water splitting. ACS Nano 2014;8:7163–9.
[21] Joo J, Chow BY, Prakash M, Boyden ES, Jacobson JM. Face-selective electrostatic control of hydrothermal zinc oxide nanowire synthesis. Nat Mater 2011;10:596–601.
[22] Dasgupta NP, Sun JW, Liu C, Brittman S, Andrews SC, Lim J, et al. 25th anniversary article: semiconductor nanowires synthesis, characterization, and applications. Adv Mater 2014;26:2137–84.
[23] Ramay SM, Atiq S, Saleem M, Mahmood A, Siddiqi SA, Naseem S, et al. Enhanced magnetization of sol-gel synthesized Pb-doped strontium hexaferrites nanocrystallites at low temperature. J Nanomater 2014;2014:452468.
[24] Shannon RD. Revised effective ionic-radii and systematic studies of interatomic distances in halides and chalcogenides. Acta Crystallogr A 1976;32:751–67.
[25] Qiu ZW, Yang XP, Han J, Zhang P, Cao BQ, Dai ZF, et al. Sodium-doped ZnO nanowires grown by high-pressure PLD and their acceptor-related optical properties. J Am Ceram Soc 2014;97:2177–84.
[26] Liu CW, Chang SJ, Hsiao CH, Lo KY, Kao TH, Wang BC, et al. Noise properties of low-temperature-grown Co-doped ZnO nanorods as ultraviolet photodetectors. IEEE J Sel Top Quant 2014;20:3800707.
[27] Chiu SH, Huang JCA. Chemical bath deposition of ZnO and Ni doped ZnO nanorod. J Non Cryst Solids 2012;358:2453–7.
[28] Ma PY, Wu Y, Fu ZY, Wang WM. Solution-based doping of cobalt into ZnO nanorods membrane. Adv Mater Res 2011;328–330:1198–201.
[29] Fukumura T, Jin ZW, Ohtomo A, Koinuma H, Kawasaki M. An oxide-diluted magnetic semiconductor: Mn-doped ZnO. Appl Phys Lett 1999;75:3366–8.
[30] Inamdar DY, Lad AD, Pathak AK, Dubenko I, Ali N, Mahamuni S. Ferromagnetism in ZnO nanocrystals: doping and surface chemistry. J Phys Chem C 2010;114:1451–9.
[31] Tahir AA, Ehsan MA, Mazhar M, Wijayantha KGU, Zeller M, Hunter AD. Photoelectrochemical and photoresponsive properties of Bi_2S_3 nanotube and nanoparticle thin films. Chem Mater 2010;22:5084–92.
[32] Jin ZW, Fukumura T, Kawasaki M, Ando K, Saito H, Sekiguchi T, et al. High throughput fabrication of transition-metal-doped epitaxial ZnO thin films: a series of oxide-diluted magnetic semiconductors and their properties. Appl Phys Lett 2001;78:3824–6.
[33] Kim KJ, Park YR. Spectroscopic ellipsometry study of optical transitions in Zn1-xCoxO alloys. Appl Phys Lett 2002;81:1420–2.
[34] John S, Soukoulis C, Cohen MH, Economou EN. Theory of electron band tails and the urbach optical-absorption edge. Phys Rev Lett 1986;57:1777–80.
[35] Cai L, Ren F, Wang M, Cai G, Chen Y, Liu Y, et al. V ions implanted ZnO nanorod arrays for photoelectrochemical water splitting under visible light. Int J Hydrogen Energy 2015;40:1394–401.
[36] Parmar KPS, Kang HJ, Bist A, Dua P, Jang JS, Lee JS. Photocatalytic and photoelectrochemical water oxidation over metal-doped monoclinic $BiVO_4$ photoanodes. ChemSusChem 2012;5:1926–34.
[37] Chen ZB, Jaramillo TF, Deutsch TG, Kleiman-Shwarsctein A, Forman AJ, Gaillard N, et al. Accelerating materials development for photoelectrochemical hydrogen production: standards for methods, definitions, and reporting protocols. J Mater Res 2010;25:3–16.
[38] Mora-Sero I, Fabregat-Santiago F, Denier B, Bisquert J, Tena-Zaera R, Elias J, et al. Determination of carrier density of ZnO nanowires by electrochemical techniques. Appl Phys Lett 2006;89:203117.
[39] Moniz SJA, Zhu J, Tang JW. 1D Co-Pi modified BiVO4/ZnO junction cascade for efficient photoelectrochemical water cleavage. Adv Energy Mater 2014;4:1301590.
[40] Moniz SJA, Tang JW. Charge transfer and photocatalytic activity in CuO/TiO_2 nanoparticle heterojunctions synthesised through a rapid, one-pot, microwave solvothermal route. ChemCatChem 2015;7:1659–67.

Please cite this article in press as: Lee WC, et al., Enhanced photoelectrochemical water oxidation by Zn_xM_yO (M = Ni, Co, K, Na) nanorod arrays, International Journal of Hydrogen Energy (2015), http://dx.doi.org/10.1016/j.ijhydene.2015.09.116